Astron. Astrophys. 361, 901–912 (2000)

ASTRONOMY
AND
ASTROPHYSICS

Strong spectral variability in NGC 7603 over 20 years⋆

W. Kollatschny[1,2], **K. Bischoff**[1], **and M. Dietrich**[3]

[1] Universitäts-Sternwarte Göttingen, Geismarlandstrasse 11, 37083 Göttingen, Germany
[2] Department of Astronomy and McDonald Observatory, University of Texas at Austin, Austin, TX 78712, USA
[3] Department of Astronomy, University of Florida, 211 Bryant Space Center, Gainesville, FL 32611-2055, USA

Received 14 June 2000 / Accepted 21 July 2000

Abstract. We present results of a long-term optical variability campaign on the Seyfert 1 galaxy NGC 7603 over a period of nearly 20 years. The optical continuum and the Balmer and Helium lines varied by a factor of 5 to 10 in this broad-line Seyfert 1 galaxy. Furthermore, it is remarkable that the optical FeII line blends varied with the same amplitude as the Hα and HeI lines. During the first half of the campaign (until 1990) there was a strong correlation between Balmer decrement variations, Hβ intensity variations and emission line asymmetry. This behaviour changed afterwards when the Hβ line intensity was higher than on average.

Key words: line: profiles – galaxies: individual: NGC 7603 – galaxies: Seyfert

1. Introduction

During the last decade much effort was spent on studying the flux variations of Seyfert 1 galaxies and quasars. Based on the results of several multifrequency variability campaigns a more sophisticated picture of the broad-line region (BLR) emerged (cf. reviews by Peterson 1993; Netzer & Peterson 1997).

In the late 70s we started a long-term variability monitoring project for dedicated AGNs to study the continuum and emission line intensity variations as well as line profile variations. NGC 7603 is one of our prime targets in this program. The nearby Seyfert 1 galaxy NGC 7603 (Mrk 530, Arp 92; z=0.0295) has an apparent magnitude of m_V=14.04 mag (de Vaucouleurs et al. 1991) corresponding to M_V=-21.3 mag (H_o=75 km s^{-1} Mpc^{-1}, q_o=0).

NGC 7603 was under debate for some time regarding a possible physical connection to a companion, NGC 7603B, of much larger redshift (z=0.0569) (Arp 1971; Sharp 1986) (see Fig. 1). The inner regions of this spiral galaxy are fairly regular. But, there are strong outer irregularities indicating past tidal interaction and/or merging events. The outer regions show boxy isophotes as well as weak tidal arms leading to the north-west and very extended arms starting to the south and extending to the west and north crossing the background galaxy NGC 7603B; it is not established that this is a real physical connection instead of a projection effect.

After the initial detection of line variability in this galaxy by Kopylov et al. (1974) and by Tohline & Osterbrock (1976) based on observations in Nov. 1974, Nov. 1975, and Feb. 1976 there were two early variability campaigns of the continuum and Hβ intensity variations from 1974 through 1987 (12 epochs) by Goodrich (1989) and from 1979 through 1982 (9 epochs) by Rosenblatt et al. (1994).

The main intention of our monitoring project is not only to study the continuum and Hβ intensity variations but also to study the variability behaviour of as many as possible emission lines and their profile variations. There are indications that individual emission line intensities and profiles show different variability patterns e.g. in NGC 5548 (Peterson et al. 1991; Wanders & Peterson 1996; Kollatschny & Dietrich 1996), NGC 4593 (Kollatschny & Dietrich 1997), and Mrk 110 (Bischoff & Kollatschny 1999).

2. Observations and data reduction

Since 1979 we observed 39 optical spectra of NGC 7603. The majority of the observations were obtained at Calar Alto Observatory/Spain with the 2.2 m and 3.5 m telescopes. But a considerable number of spectra was recorded at La Silla, ESO/Chile with the 1.5 m, 2.2 m, and 3.6 m telescopes as well as with the 2.7 m telescope at McDonald Observatory/USA. The early observations taken with the ESO 1.5 m telescope from 1979 until 1985 were performed with an IDS detector. From 1986 onward we used different CCD detectors (RCA, GEC, Tektronix). In most cases Boller & Chivens spectrographs were attached to the telescope. But in June 1992, Dec. 1993, and Aug. 1996 focal reducers including grisms were attached to the 3.5 m and 2.2 m telescopes at Calar Alto Observatory.

The IDS attached to the 1.5 m telescope had an aperture of 4″ x 4″. For observations in the long slit mode we used spectrograph slit configurations with projected widths of 2″ to 2″.5 and 2′ length under typical seeing conditions of 1″ to 2″.

The observing dates and corresponding Julian Dates together with the used telescopes and exposure times are listed in Table 1.

Send offprint requests to: W. Kollatschny (wkollat@uni-sw.gwdg.de)

⋆ Based on observations taken at the German-Spanish Astronomical Centre Calar Alto, ESO, and McDonald Observatory

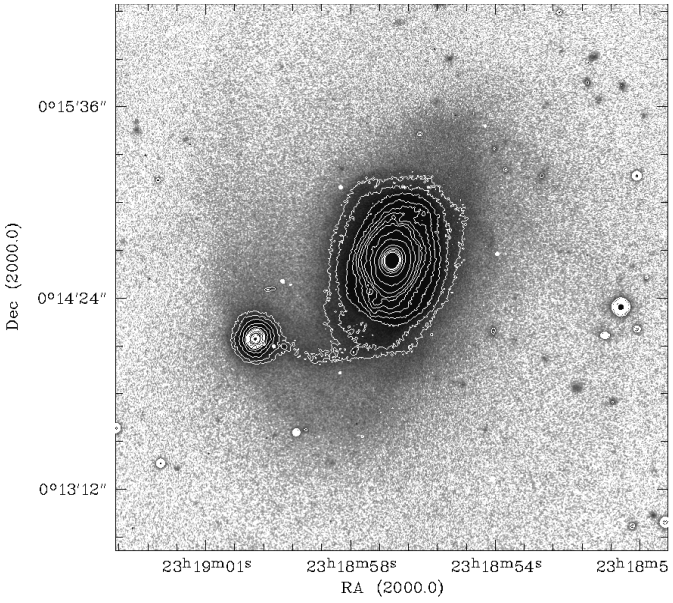

Fig. 1. Optical R-band image of NGC 7603. North is up, east is to the left.

The reduction of the spectra, i.e. bias correction, flatfield correction, wavelength calibration, night sky subtraction and flux calibration, was done in a homogeneous way using the ESO MIDAS[1] package. We extracted spectra of the central 5″. Our optical spectra typically cover a wavelength range from 4000 Å to 7200 Å with a spectral resolution of 3 to 7 Å per pixel. The Hβ and [OIII]λ4959,5007 lines were covered in all our spectra.

The absolute calibration of the NGC 7603 spectra was achieved by scaling the [OIII]λ5007 line of all spectra to those obtained under photometric conditions. We derived an absolute flux of F([OIII]λ5007) = (36.0$\pm$3.0) 10^{-15} erg s^{-1} cm^{-2} ($\lambda\lambda$5150 - 5170 Å observed frame). This agrees within an error of 3 % with the value given by Goodrich (1989) who measured F([OIII]λ5007) = 35.0 10^{-15} erg s^{-1} cm^{-2}.

Furthermore, we corrected all our data for small spectral shifts and resolution differences with respect to a mean reference spectrum using an automatic scaling program of van Groningen & Wanders (1992).

To investigate the spatial extension of the narrow-line region (NLR) we took spectra at different position angles. The [OIII]λ5007 emission line flux was always spatially unresolved.

Furthermore, we took broad-band B,V,R,I and narrow-band images of NGC 7603 in the redshifted Hα and [OIII]λ5007 lines. The R-band image of NGC 7603 as shown in Fig. 1 was taken with the 2.2 m telescope at Calar Alto Observatory on September 20, 1993 with an exposure time of 15 minutes. We reduced the CCD images with the ESO MIDAS package. We measured a diameter of less than 1″ for the [OIII]λ5007 emission region. Hence, the NLR can be taken as unresolved as well as the BLR.

[1] Munich Image Data Analysis System, distributed by ESO

Table 1. Log of observations

Julian Date 2 400 000+ (1)	UT Date (2)	Telescope (3)	Exp. time [sec.] (4)
44168	1979-10-21	ESO 1.5	3600
46029	1984-11-24	ESO 1.5	4200
46030	1984-11-25	ESO 1.5	4800
46031	1984-11-26	ESO 1.5	6000
46032	1984-11-27	ESO 1.5	4800
46289	1985-08-11	ESO 1.5	1920
46292	1985-08-14	ESO 1.5	2400
46294	1985-08-16	ESO 1.5	1200
46583	1986-06-01	ESO 2.2	3600
46584	1986-06-02	ESO 2.2	2700
46966	1987-06-19	CA 3.5	1200
46973	1987-06-26	CA 3.5	1200
46974	1987-06-27	CA 3.5	1200
46975	1987-06-28	CA 3.5	840
47439	1988-10-04	CA 3.5	1200
47827	1989-10-27	CA 2.2	2700
47831	1989-10-31	CA 2.2	6600
47832	1989-11-01	CA 2.2	6600
48089	1990-07-16	CA 2.2	340
48090	1990-07-17	CA 2.2	3000
48474	1991-08-05	CA 2.2	3000
48506	1991-09-06	CA 3.5	1800
48793	1992-06-19	CA 3.5	300
48798	1992-06-24	CA 3.5	500
48814	1992-07-10	CA 3.5	1800
48860	1992-08-25	CA 2.2	3000
48862	1992-08-27	CA 2.2	3000
48864	1992-08-29	CA 2.2	3000
48866	1992-08-31	CA 2.2	3000
49237	1993-09-06	CA 3.5	900
49241	1993-09-10	CA 3.5	1800
49340	1993-12-18	CA 3.5	900
49577	1994-08-12	ESO 3.6	900
49595	1994-08-30	CA 2.2	2400
49631	1994-10-05	ESO 1.5	2400
49869	1995-05-31	MDO 2.7	900
49928	1995-07-29	MDO 2.7	750
50393	1996-11-05	ESO 2.2	900
51168	1998-12-20	CA 3.5	900

CA = Calar Alto Observatory
ESO = European Southern Observatory
MDO = McDonald Observatory

Archival snapshot images of NGC 7603 taken with the Hubble Space Telescope WFPC-2 camera in July, 1994, confirm the unresolved nuclear region in this galaxy (Malkan et al. 1998).

UV spectra taken with the IUE satellite in July 1979, August 1985, and June 1986 will be taken into consideration for comparison with our optical data.

3. Results and discussion

Some typical spectra of NGC 7603 are plotted in Fig. 2 showing the range of continuum variations as well as the strong variations

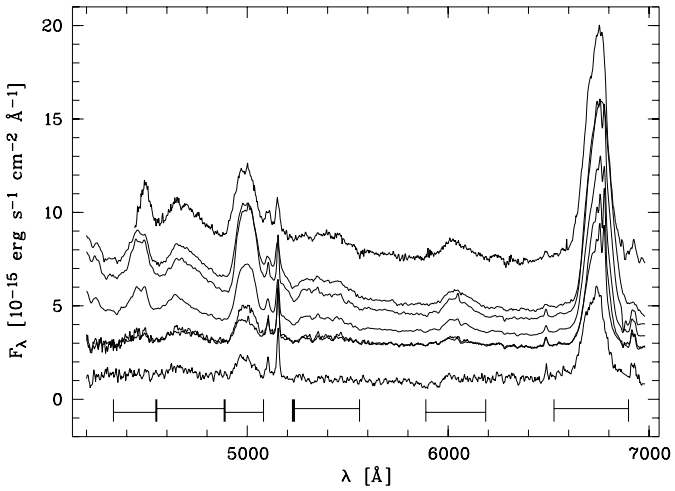

Fig. 2. Normalized spectra of NGC 7603 taken at different epochs in Oct. 79, Oct. 88, July 90, Aug. 92, Sep. 93, Dec. 93 and Dec. 98 (from bottom to top). The horizontal bars underneath the spectra show the integration range for the continuum, the Balmer and He lines, as well as FeII line blends.

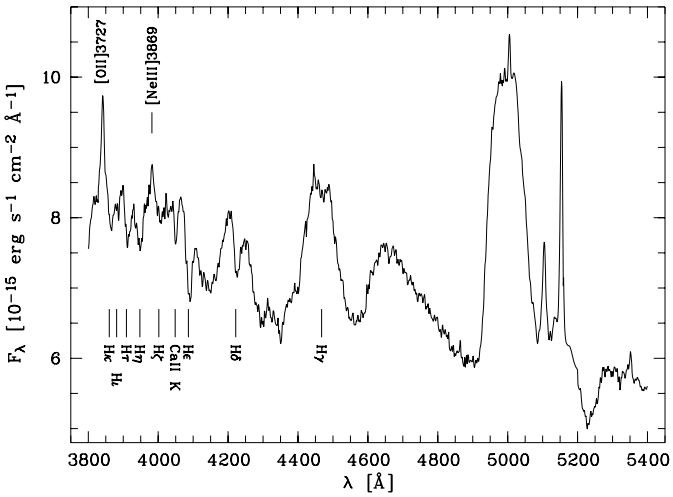

Fig. 3. Blue spectral region showing the underlying Balmer absorption lines in detail.

in the Balmer and Helium lines and broad FeII line blends. A spectrum of the blue spectral range taken in Sep. 93 is shown in Fig. 3.

The higher order Balmer lines in absorption as well as the CaII K line can be clearly identified. These are characteristics of a young stellar component as seen e.g. in the quasar FIRST J164311.3+315618 (Brotherton et al. 1999). The existence of a Balmer absorption line component in NGC 7603 has already been mentioned by Goodrich (1989).

Detailed population and evolutionary synthesis models of 2D-spectra confirm the existence of an underlying starburst component ($5 \cdot 10^6$ yr) superimposed on the AGN spectrum (Goerdt & Kollatschny 1998; Kollatschny & Goerdt 2000).

3.1. Line and continuum variations

The results of our continuum intensity measurements at λ_{rest} = 5080 Å as well as the integrated line intensities of Hα, Hβ, Hγ, HeIλ5876, and of the two strong optical FeII line blends FeII 4570 (4415 Å – 4745 Å) and FeII 5200 (5085 Å – 5400 Å) are given in Table 2. We summed up our spectra taken in 1984 and 1985 respectively to improve the S/N ratio (Table 2). These spectra have been taken with an IDS detector. They do not show any variations on time scales of days within our error limits. We combined the two spectra taken in 1986 within 1 day since one spectrum was taken in the blue spectral range and the other one in the red spectral range.

The continuum intensities are the mean values in the wavelength range given in Table 3, Column (2). Line intensities were integrated over the quoted wavelength limits after subtraction of a linear pseudo-continuum defined by the boundaries given in Column (3). All wavelengths are given in rest frame.

The individual light curves are plotted in Fig. 4. Additionally we show the continuum and Hα, Hβ intensities on a logarithmic scale including IUE UV continuum intensities at λ1300 Å and λ1830 Å (restframe) and UV line intensities of the Lyα, CIVλ1549, NVλ1240, and SiIV+OIV]λ1398 lines.

We started our observing campaign of NGC 7603 in 1979. In Table 2 and Fig. 4 we added some continuum and line intensity measurements taken by Goodrich (1989, 1995 and references therein) to extend our data basis. They are marked with an asterisk in Column 9. His measurements are in very good agreement with our data. For a direct comparison we scaled our [OIII]λ5007 flux to F([OIII] 5007) = 35.0 10^{-15} erg s^{-1} cm^{-2} (Goodrich 1989) and we added to his continuum data a stellar excess flux of 1.01 10^{-15} erg sec^{-1} cm^{-2} Å^{-1} subtracted by him before. Rosenblatt et al. (1994) took spectra of NGC 7603 at similar epochs as Goodrich (1989). But their [OIII]λ5007 intensities, [OIII]/Hβ ratios as well as continuum intensities disagree with those of Goodrich. Therefore, we did not consider these data.

In Table 4 we list statistics of our optical continuum and emission line data. Given are the maximum and minimum fluxes F_{max} and F_{min}, peak-to-peak amplitudes $R_{max} = F_{max}/F_{min}$, the mean flux over the entire period of observations $\langle F \rangle$, the standard deviation σ_F, and the fractional variation

$$F_{var} = \frac{\sqrt{\sigma_F{}^2 - \Delta^2}}{\langle F \rangle}$$

where the quantity Δ^2 is the mean square value of the uncertainties Δ_i associated with the fluxes as defined by Rodríguez-Pascual et al. (1997).

All broad emission lines in NGC 7603 show very strong variability amplitudes. For a comparison see the line variations in NGC 5548 (Dietrich et al. 1993) or in Mrk 110 (Bischoff & Kollatschny 1999) and the Hβ variations in other Seyfert galaxies (e.g. Peterson et al. 1998). For those Seyfert 1 galaxies the parameter F_{var} is of the order of less than 0.2.

The line intensity of Hβ is plotted as a function of continuum intensity at 5080 Å in Fig. 5. There is a close linear correlation between these data as expected from photoionization theory.

Table 2. Continuum and line fluxes

Julian Date 2 400 000+	F_{5080}	Hα	Hβ	Hγ	HeIλ5876	FeII 4570	FeII 5200	Remarks
(1)	(2)	(3)	(4)	(5)	(6)	(7)	(8)	(9)
42359	2.66 ±0.30	773. ±140	171. ±30.	75 ±13	55.7±10.0	87.0±16.		*
42392	2.18 ±0.15		123. ±22.					*
42726	1.50 ±0.12	390. ±60.	56.0 ±11.					*
42812	1.46 ±0.12		51.0 ±9.2					*
42951	1.58 ±0.12		63.0 ±11.					*
42987	1.47 ±0.12		52.0 ±9.3					*
43024	1.85 ±0.15		90.0 ±16.					*
43056	1.50 ±0.12		55.0 ±11.					*
44168	1.03 ±0.15	652. ±26.	113. ±7.0	11 ± 4	30.2± 8.0	63.6±7.0	35.1 ±8.0	1
44911	2.57 ±0.14	749. ±70.	162. ±15.					*
45592	2.46 ±0.15	731. ±66.	151. ±13.					*
45653	2.73 ±0.15		178. ±15.					*
46031	4.17 ±0.12		275. ±8.0			116.3±6.0	80.3 ±5.0	2
46292	4.04 ±0.12	924. ±37.	284. ±8.0		55.9± 3.5		83.2 ±5.0	3
46584	4.24 ±0.16	745. ±30.	213. ±6.6	82 ± 4	61.0± 3.5	140.4±6.0	83.9 ±5.0	4
46966	3.27 ±0.12	824. ±33.	203. ±6.1	77 ± 4	58.8± 3.5	129.9±5.2	84.4 ±4.2	5
46973	3.08 ±0.12	805. ±32.	189. ±5.7	73 ± 4	52.9± 3.5	110.2±4.4	76.8 ±4.0	6
46974	3.07 ±0.12	801. ±32.	192. ±5.8	73 ± 4	50.1± 3.5	111.1±4.4	75.0 ±4.0	7
46975	2.96 ±0.12	785. ±31.	193. ±5.8	72 ± 4	49.9± 3.5	111.8±4.4	75.7 ±4.0	8
47002	2.58 ±0.20	772. ±69.	163. ±12.		53.4± 5.3			*
47439	3.11 ±0.12	747. ±50.	144. ±4.4	61 ± 4	43.3± 3.5	123.6±4.9	71.6 ±4.0	9
47827	3.31 ±0.20	726. ±45.	147. ±4.4	74 ± 5	41.5± 6.0	157.3±6.3	73.5 ±4.5	10
47832	3.26 ±0.12		158. ±4.8					11
48090	3.17 ±0.12	918. ±37.	210. ±6.3	93 ± 5	46.3± 3.5	153.9±6.2	77.1 ±4.0	12
48474	4.36 ±0.16	1503 ±60.	373. ±11.	145 ± 7	93.8± 3.8	201.0±8.0	113. ±4.5	13
48506	3.78 ±0.12	1165 ±47.	223. ±6.7	85 ± 4	65.3± 3.5	174.1±7.0	105. ±4.2	14
48793	3.10 ±0.19	1047 ±42.	220. ±6.6	80 ± 4	68.1± 3.5	157.3±6.3	96.8 ±4.1	15
48798	3.09 ±0.19		233. ±7.0					16
48814	4.63 ±0.17	1145 ±46.	333. ±10.	159 ± 8	102.5± 4.2	187.3±7.5	115. ±4.6	17
48860	4.46 ±0.17	1242 ±50.	361. ±11.	151 ± 8	88.2± 3.5	181.7±7.3	147. ±5.9	18
48862	5.09 ±0.18	1229 ±49.	386. ±12.	166 ± 8	88.2± 3.5	207.8±8.3	132. ±5.3	19
48864	3.94 ±0.15	1128 ±45.	336. ±10.	157 ± 8	83.3± 3.5	190.4±7.6	126. ±5.0	20
48866	3.32 ±0.14	989. ±40.	284. ±8.5	122 ± 6	65.8± 3.5	148.7±6.0	106. ±4.3	21
49237	5.22 ±0.18	1567 ±63.	496. ±15.	229 ±11	125.6± 5.0	240.8±9.6	179. ±7.2	22
49241	5.44 ±0.19	1541 ±62.	518. ±15.	228 ±11	141.4± 5.6	263.6±10.	164. ±6.6	23
49270	6.37 ±0.21	1862 ±93.	541. ±27.		146.0± 7.3			*
49340	6.15 ±0.21	1584 ±63.	451. ±14.	187 ± 9	113.7± 4.6	223.9±9.0	162. ±6.5	24
49577	4.77 ±0.14	1207 ±48.	397. ±12.	207 ±10	96.0± 3.8	260.9±10.	165. ±6.6	25
49595	4.76 ±0.14	1175 ±46.	362. ±11.		94.1± 3.8	257.7±10.	154. ±6.2	26
49631	3.87 ±0.13	801. ±32.	252. ±7.6	130 ± 6	67.6± 3.5	184.9±7.4	124. ±5.0	27
49869	4.02 ±0.13	1063 ±43.	267. ±8.0		72.9± 3.5		136. ±5.4	28
49928	4.59 ±0.14		267. ±8.0	125 ± 6		205.8±8.0		29
50393	6.07 ±0.21	1453 ±62.	432. ±13.	199 ±10	127.1± 5.1	269.3±10.	164. ±6.6	30
51168	8.77 ±0.29	1691 ±68.	445. ±13.		164.4± 6.6	288.8±12.	178. ±7.1	31

Continuum fluxes (2) in 10^{-15} erg sec^{-1} cm^{-2} Å^{-1}
Line fluxes (3) - (8) in 10^{-15} erg sec^{-1} cm^{-2}

The small scatter can easily be explained by the delay of the Hβ intensity variations with respect to the ionizing continuum variations. The data point with the largest continuum value was taken at the end of the observing campaign in Dec. 1998.

In Fig. 6 we plot the intensity of HeIλ5876 as a function of Hβ. Again, there is a close correlation.

The intensity of the FeIIλ5200 line blend is shown as a function of the Hβ intensity in Fig. 7. There is a larger scatter in comparison to the HeIλ5876/Hβ relation (Fig. 6). This might be explained by a different delay of the FeII lines with respect to continuum variations compared to the Hβ line.

The relationship of the FeIIλ4570 line blend with respect to Hβ is not shown explicitly. The behaviour is the same as that of the FeIIλ5200 line blend.

In most other Seyfert galaxies the variations of the optical FeII blends are much weaker in comparison to other optical emission lines or not detectable at all (e.g. Maoz et al. 1993). In the narrow-line Seyfert 1 galaxy Mrk 110 the optical FeII line

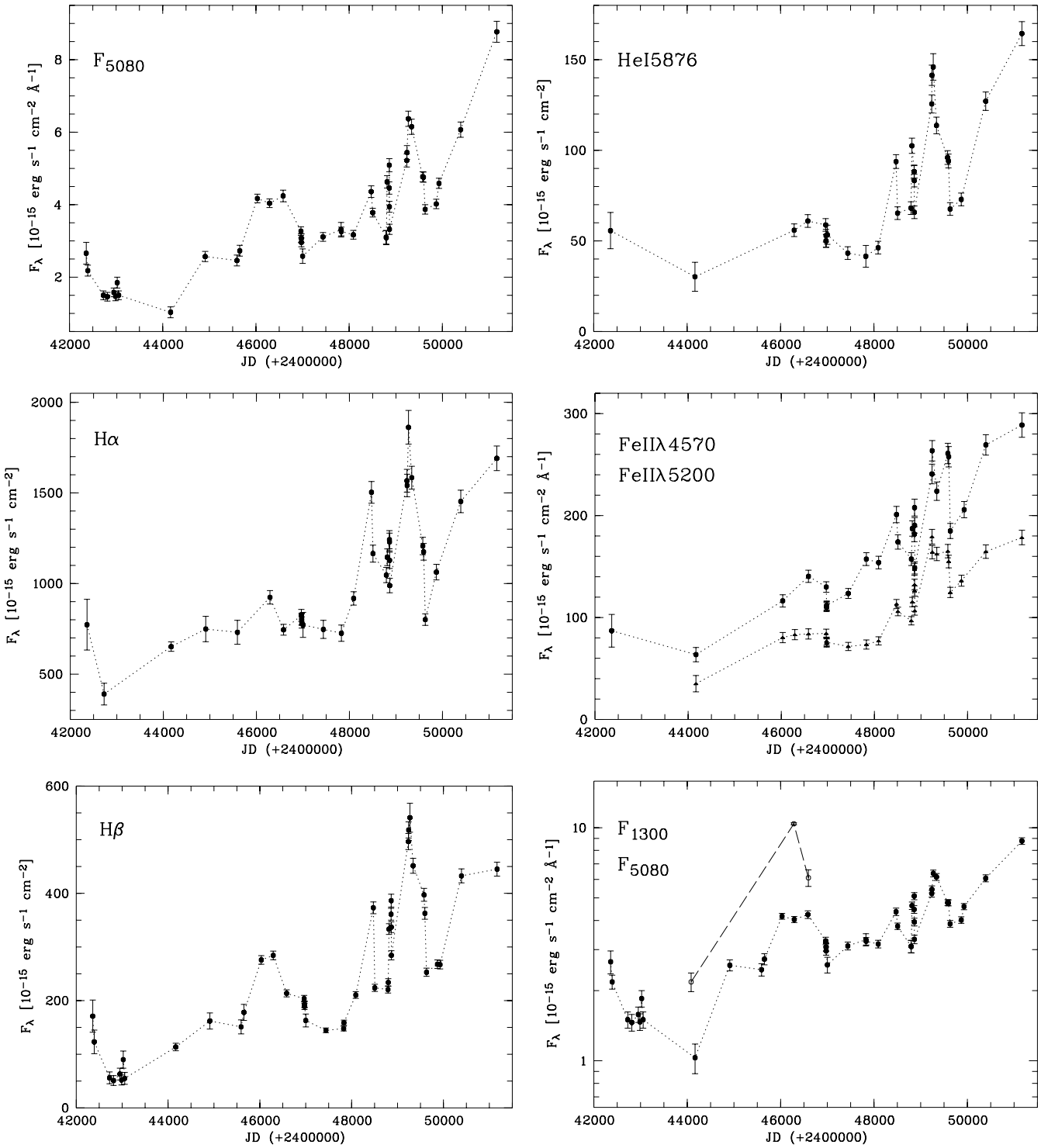

Fig. 4. Light curves of continuum flux at λ_{rest}=5080 Å and integrated emission line intensities of Hα, Hβ, Hγ HeIλ5876, and FeII 4570 (upper curve) and FeII 5200 Å (lower curve). The points are connected to aid the eye. At the bottom to the right we plotted the Hα and Hβ light curves on a logarithmic scale. In addition we draw in the same plot the UV line intensities of CIVλ1549, Lyα, NVλ1240, and SiIV+OIV]λ1398 (from top to bottom). Above of this plot the optical continuum and the UV continuum are shown on a logarithmic scale.

flux remained constant within an error of 10 % over 10 years (Bischoff & Kollatschny 1999) even though the continuum and the Balmer lines varied by a factor of 2 to 5. In a monitoring program on Narrow-Line Seyfert 1 Galaxies Giannuzzo & Stirpe (1996) reported FeIIλ5200 line variations of less than 15 % only (with one exception) compared to Hβ variations of the order of 30 %. In the Seyfert galaxy NGC 5548 no significant FeII variations (less than 20 %) have been detected (Dietrich et al. 1993).

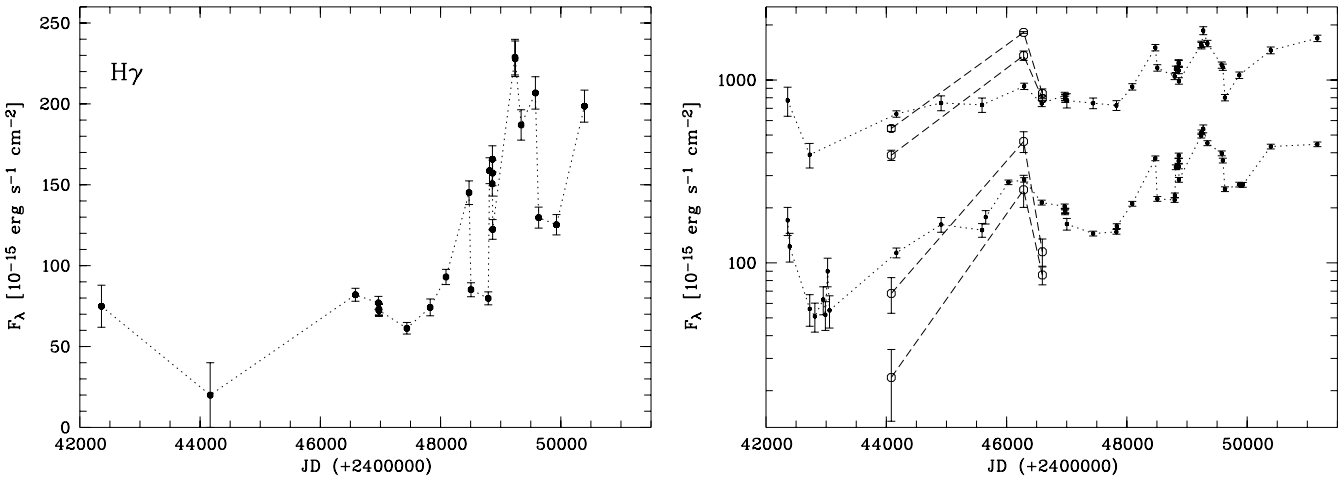

Fig. 4. (continued)

Table 3. Extraction windows of the continuum and emission line flux integrations

Cont./Line (1)	Wavelength range (2)	Pseudo-continuum (3)
F_{5080}	5075 Å – 5085 Å	
Hγ	4210 Å – 4415 Å	4210 Å – 4745 Å
FeII 4570	4415 Å – 4745 Å	4210 Å – 4745 Å
Hβ	4745 Å – 4935 Å	4745 Å – 5080 Å
FeII 5200	5085 Å – 5400 Å	5080 Å – 5400 Å
HeIλ5876	5720 Å – 6010 Å	5720 Å – 6010 Å
Hα	6340 Å – 6700 Å	6270 Å – 6785 Å

Table 4. Variability statistics

Line (1)	F_{max} (2)	F_{min} (3)	R_{max} (4)	$\langle F \rangle$ (5)	σ_F (6)	F_{var} (7)
F_{5080}	8.77	1.03	7.74	3.61	1.55	0.427
Hα	1862.	390.	4.77	1052.	351.	0.329
Hβ	541.	51.0	10.61	246.	133.	0.538
Hγ	228.9	10.8	21.20	122.	58.2	0.472
HeIλ5876	164.4	30.2	5.44	80.1	34.5	0.426
FeII 4570	288.8	63.6	4.54	177.	60.0	0.337
FeII 5200	179.3	35.1	5.11	114.	39.4	0.343

Continuum fluxes in 10^{-15} erg sec^{-1} cm^{-2} Å^{-1}
Line fluxes in 10^{-15} erg sec^{-1} cm^{-2}

Variations in the FeIIλ4570 line blend are mainly ascribed to HeIIλ4686 variations in that wavelength interval (Kollatschny & Dietrich 1996). On the other hand in the broad-line Seyfert 1 galaxies Akn 120 (Kollatschny et al. 1981) and Fairall 9 (Kollatschny and Fricke 1985) considerable FeII variations (larger than 50 %) have been detected. It might be worth to extend optical variability campaigns on larger Seyfert samples with different broad line widths to investigate the validity of the trend that optical FeII variability amplitudes are stronger in broad-line Seyfert 1 galaxies - independently of the Hβ variations.

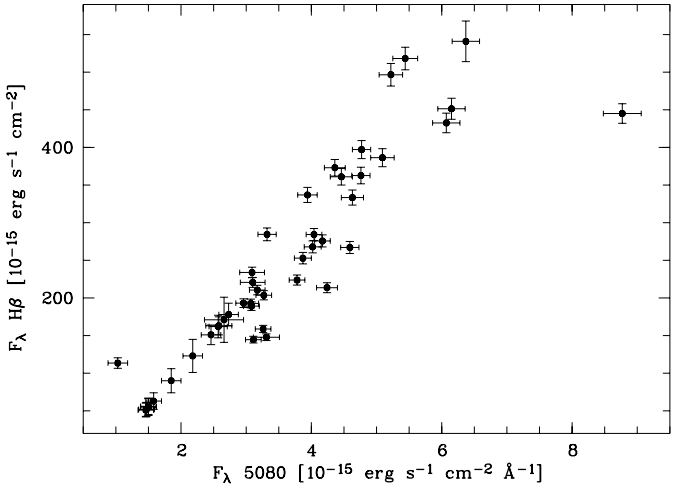

Fig. 5. Line intensity of Hβ as a function of the continuum flux at 5080 Å for all observing epochs listed in Table 2.

3.2. UV spectra

Three UV SWP spectra of NGC 7603 haven been taken with the IUE satellite on July 28, 1979, August 5, 1985, and June 12, 1986. These spectra have been taken within at most a few months with respect to our optical spectra. An additional IUE spectrum - taken in November 1979 - is not taken into account since the nucleus was not centered properly in the IUE aperture. The IUE spectra of NGC 7603 are shown in Fig. 8. The geocoronal Lyα line has been removed. The intensities of the Lyα, NVλ1240, SiIV+OIV]λ1398 and CIVλ1549 lines and the continuum at λ1300 and λ1830 (restframe) are given in Table 5.

There are strong variations by a factor of 3 to 10. The high excitation lines are the most variable ones. The red wing of Lyα seems to be more variable than the blue wing. But, this might be affected by blending with the NVλ1240 line.

The CIVλ1549 line is slightly broader than Lyα. The Lyα to CIVλ1549 line ratio is unusually small. This has been first noticed in the spectrum taken in 1979 (Clavel & Joly 1984).

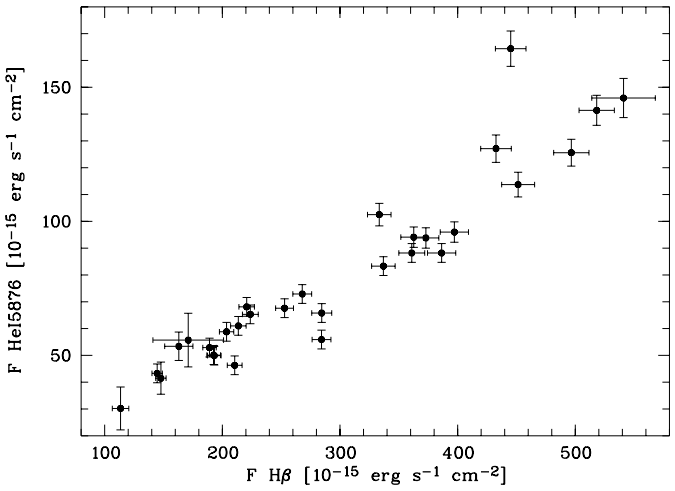

Fig. 6. Line intensity of HeIλ5876 as a function of Hβ intensity.

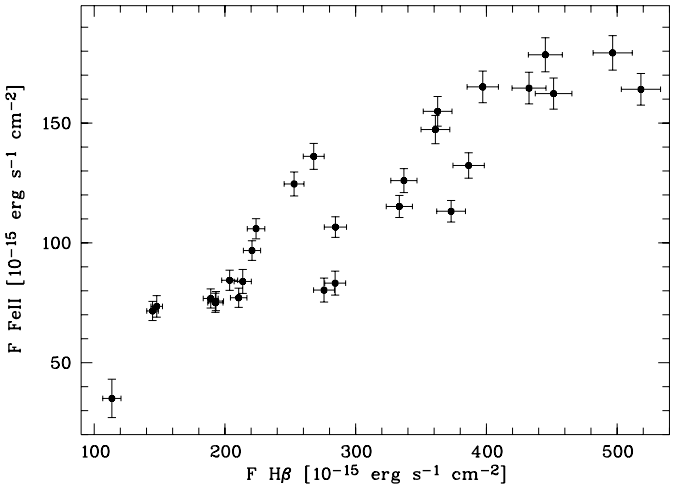

Fig. 7. FeIIλ5200 intensity as a function of Hβ line intensity.

The HeIIλ1640 line is not detectable. We can estimate only an upper limit in the IUE spectrum of F(HeII1640) = $30 \cdot 10^{-15}$ erg sec^{-1} cm^{-2}. On the other hand there are FeII lines of the multiplets 40, 41 and 38, 84, 85 to be seen in the UV. This corresponds to the strong optical FeII line blends.

We calculated Lyα/Hβ ratios of 3.4, 4.8, and 3.7 for the three epochs. This is far below the mean Lyα/Hβ value of 6.8 for Seyfert 1 galaxies (Wu et al. 1983) and might be an indication for internal dust absorption.

3.3. CCF analysis

We correlated the continuum light curve with the emission line light curves using an interpolation cross-correlation function method (Gaskell & Peterson 1987) and a more sophisticated interpolation scheme of constructing equally-sampled light curves from unequally-sampled data (Welsh et al. 2000; Rybicki & Press 1992). But we could not determine any significant delay of the emission line light curves with respect to the continuum. Subsamples led to the same result. An obvious explanation is

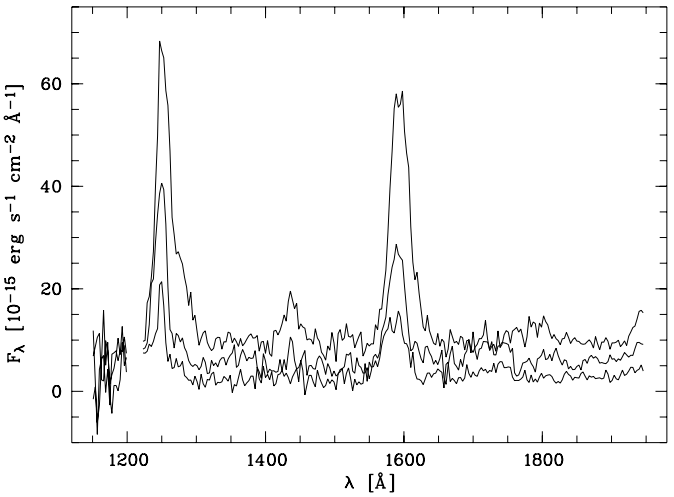

Fig. 8. Short wavelength IUE UV spectra of NGC 7603 taken in July 1979 (bottom), August 1985 (top), and June 1986.

the poor temporal sampling of the light curves. On the other hand the sampling was not worse compared to the light curves of Mrk 110 (Bischoff & Kollatschny 1999). As will be shown later the case of NGC 7603 might be more complicate since there might be additional optical depth effects or dust variations significant.

3.4. Line profile shapes and variations

We calculated mean and rms profiles of the strong broad emission lines in NGC 7603 (Table 6). The rms profiles are a measure of the variable part in the individual line profiles. The normalized mean and rms profiles of Hα, Hβ, HeIλ5876, and Lyα are shown in Fig. 9. We normalized the line profiles with respect to their central intensity. The mean and rms profiles of the individual lines are different with respect to their shape and full width at half maximum (FWHM). In Table 6 we list the widths of the mean and rms profiles.

The UV line profiles of Lyα and CIVλ1549 have been calculated from the three observed spectra only. The red wing of the Lyα rms profile (Fig. 9) is strongly contaminated by the NVλ1240 line. The broad shoulder in the red wing of Lyα at $v_{rel} \simeq 6200$ km s^{-1} can be attributed to the NVλ1240 line. The mean profiles of Hα and Lyα are significantly narrower than the profile of Hβ while the widths of their rms spectra are of the same order. In the same sense the rms spectra of the high excitation lines (e.g. CIV) show the same width as the low excitation lines. Generally, there is a trend that the higher ionized lines showing the largest variability amplitudes and originating closer to the central ionizing continuum source show the broadest rms line profiles as in NGC 5548 (Peterson 1993; Dietrich et al. 1993) or in Mrk 110 (Bischoff & Kollatschny 1999). This trend is not to be seen in NGC 7603.

The maxima in the red wings of the rms line profiles are systematically higher (≈10%) in the Hα, Hβ, and HeIλ5876 lines with respect to the blue wings (Fig. 9). This indicates that the variability amplitudes in the red wings are systemat-

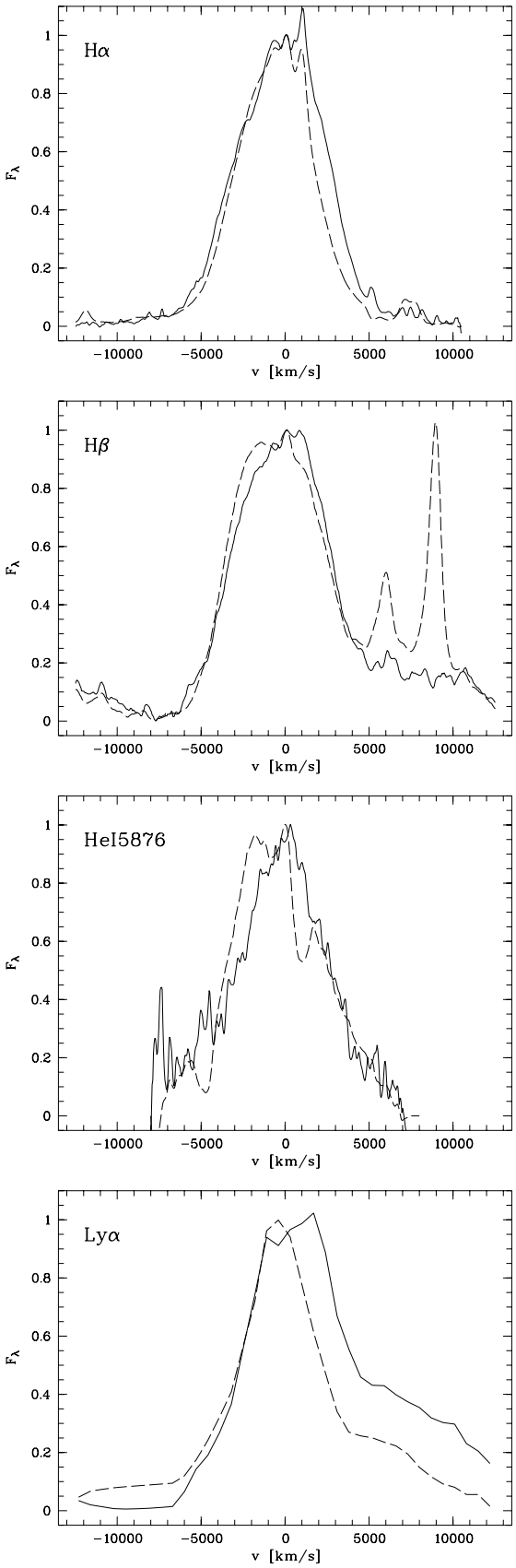

Fig. 9. Mean (dashed lines) and rms (solid lines) profiles of Hα, Hβ, HeIλ5876, and Lyα.

Table 6. Mean and rms line widths (FWHM)

Line	FWHM(mean) [km s^{-1}]	FWHM(rms) [km s^{-1}]
(1)	(2)	(3)
Hα	5060 $\pm$ 100	6350 $\pm$ 100
HeIλ5876	6200 $\pm$ 200	5700 $\pm$ 200
Hβ	6560 $\pm$ 100	6470 $\pm$ 100
CIVλ1549	6170 $\pm$ 200	6100 $\pm$ 300
Lyα	5010 $\pm$ 200	6900 $\pm$ 300

ically stronger. The same general trend has been observed in other Seyfert galaxies e.g. in NGC 5548 (Kollatschny & Dietrich 1996), NGC 4593 (Kollatschny & Dietrich 1997), and Mrk 110 (Bischoff & Kollatschny 1999).

Mean Hβ line profiles averaged over periods of years are plotted in Fig. 10. They give the long-term trend of the line asymmetry. They clearly show that for the first 8 years of the variability campaign (1979–1987) the blue Hβ line wing was far more intense than the red one. The line asymmetry decreased from 1988 until 1990 and remained of the same order subsequently when the overall line intensity increased. The Hα profiles show the same basic trend. The long-term line asymmetry variations are best to be seen in the asymmetry-intensity plots of the Hα and Hβ profiles (Fig. 11). The asymmetry is defined by the intensity ratio of the blue wing ($v_{rel} = -5000 \ldots -500$ km s^{-1}) and the red wing ($v_{rel} = +500 \ldots +5000$ km s^{-1}). The numbers in the plots denote the observing epochs (Table 2, remarks). Hα values are not available for all Hβ observing epochs (see Table 2). The Hα and Hβ line profiles show the same general trend that the asymmetry was stronger when the line intensity was lower with a more pronounced red wing.

The rms profiles of the Hα and Hβ lines clearly show substructures. The S/N ratio in the HeIλ5876 line is not sufficient to make a clear statement. Besides a central component there are two inner components in Hα and Hβ at $v_{rel} = +1050 \pm 50$ km s^{-1} and $v_{rel} = -750 \pm 50$ km s^{-1}. These components are close to the [NII]λ6548,6583 lines in the Hα line. Hence, it is important that they are present in Hβ, too. Furthermore, there are two outer components in the Hα and Hβ lines at $v_{rel} = +2000 \pm 100$ km s^{-1} and at about $v_{rel} = -2000 \pm 200$ km s^{-1}. Goodrich (1989) mentioned internal structures in the Hβ line at v_{rel}= -2500 and +1000 km s^{-1} when he subtracted NGC 7603 spectra taken in 1981 and 1983.

Inner line components at similar radial velocities as in NGC 7603 have been found in the rms line profiles of the variable Seyfert galaxy NGC 4593 (Kollatschny & Dietrich 1997).

The Hγ line is not shown because of its lower S/N ratio and its severe blending with the [OIII]λ4363 line. The HeIλ5876 line (Fig. 9) is influenced by NaD absorption of the host galaxy.

Both optical FeII line blends (see Figs. 2,3 and Table 3) do not show any pronounced internal structures in the mean and rms spectra. The variations occur uniformly over the whole blend. Therefore, the mean and their respective rms profiles are identical. The variations in the Hβ complex (Fig. 9) at $v_{rel} =$

Table 5. UV continuum and integrated line fluxes

Julian Date 2 400 000+	F_{1300}	F_{1830}	Lyα	N vλ1240	Si IVλ1396+ O IV] λ1402	C IVλ1550
(1)	(2)	(3)	(4)	(5)	(6)	(7)
44083	2.18 ±0.2	2.92 ±0.2	388. ±25.	68. ±15.	23.6±10.	543. ±20.
46283	10.4 ±0.1	9.82 ±0.2	1360 ±80.	461. ±60.	251.0±50.	1820 ±20.
46595	6.10 ±0.5	6.11 ±0.2	793. ±25.	115. ±20.	85.8±10.	844. ±50.

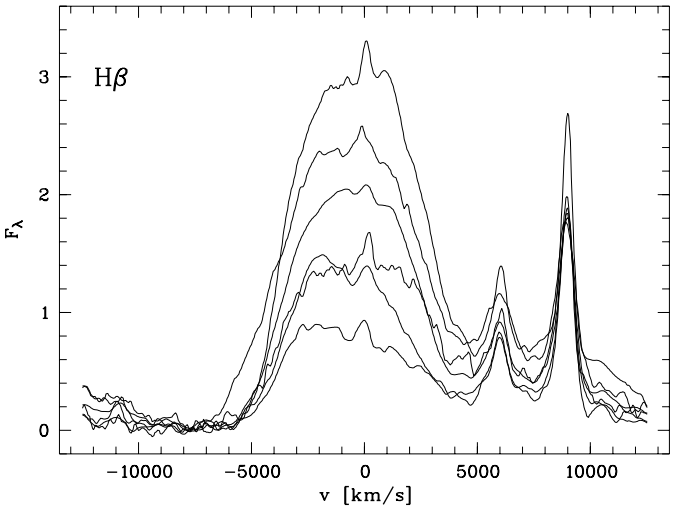

Fig. 10. Mean Hβ line profiles averaged over different epochs. From bottom to top: 1988–89; 1979–87; 1994–95; 1990–92; 1996–98; maximum taken at Sep. 93.

$+5000 \ldots + 13000\,\mathrm{km\,s^{-1}}$ underneath the [OIII]λ4959,5007 lines might be attributed to FeII variations, too.

3.5. Balmer decrement

We calculated the Balmer decrement for all observing epochs. Fig. 12 shows the variation of the Balmer decrement as a function of time. For comparison we display a scaled Hβ light curve in the same figure at the bottom. The pattern of the Balmer decrement variations follows closely the Hβ light curve until July, 1992 (JD 2 448 814). Afterwards there were still strong line intensity variations but the Balmer decrement varied now with a much smaller amplitude.

The numerical values of the Balmer decrement span the range from 3.0 to 7.0. We did not correct the Hα intensity for the contribution of the [NII] lines. Therefore, the intrinsic Hα/Hβ line intensity ratio might be lower by up to 5 %. Simple photoionization calculations (case B, i.e. large optical depth approximation) result in a value of 2.8 for the Hα/Hβ line ratio (e.g. Osterbrock 1977).

In Fig. 13 we plot the Balmer decrement Hα/Hβ as a function of Hβ intensity. The numerical values are connected by a solid line from the beginning of the campaign until July, 1990 (JD 2 448 090) and by a dashed line from July, 1992 (JD 2 448 814) on; the values in the intervening period of two years are connected by a dotted line. There is a linear anti-correlation of the Balmer decrement with the Hβ intensity until July, 1990 when the Balmer decrement values were high and the Hβ intensities were low. Towards the end of our campaign - after July, 1992 - the Balmer decrement remained nearly constant within the parameter range of 3 to 4 independently from the Hβ intensity which was high during this period.

While the Balmer decrement in NGC 7603 varies from 3.0 to 7.0 it ranges e.g. between 4.2 and 6.3 in NGC 5548 (Wamsteker et al. 1990) and between 3.2 and 4.2 in Mrk 110 (Bischoff & Kollatschny 1999) only.

Theoretical photoionization models show that the relative intensities of the hydrogen lines in AGNs might depend in a complicated way on temperature, density, optical depth and/or collisional excitation effects. In addition wavelength dependent dust absorption may play an important role.

We tried to estimate the amount of dust independently. But the line ratio HeIIλ4686/HeIIλ1640 could not be used as a dust indicator due to faintness of these emission lines and their blending with other lines. Variations of the continuum slope could provide additional hints on dust absorption. In Fig. 2 one can see that the underlying continuum in NGC 7603 became bluer with increasing intensity. This can be easily explained by the major importance of the blue ionizing continuum flux in higher intensity stages with respect to the host galaxy spectrum. The slope variation is not necessarily caused by changing dust absorption.

In Fig. 14 we plot the Hα/Hβ/Hγ line ratios for all epochs. The open square shows the standard recombination ratio (case B). The dashed line shows the effect of interstellar extinction. The observed Balmer line intensity ratios in NGC 7603 are compatible with variable extinction.

But the variation of the Balmer decrement as a function of the ionizing continuum flux could be explained by radiative transfer effects rather than by variation of dust extinction. An increased optical depth in the Balmer lines can be induced by an increasing ionizing flux since the ionization front penetrates deeper into the gas in a radiation-bounded system. Model calculations by Davidson & Netzer (1979) show that the Hα/Hβ ratio varies depending on optical depth. However the Hβ/Hγ ratio remains nearly independent from optical depth. The data in Fig. 14 can not exclude this explanation unambiguously.

Furthermore, ionizing flux variations by itself can explain the largest variations in Lyα and the decreasing amplitudes in Hγ, Hβ and Hα (Tables 4, 5) without invoking changes in density (Wamsteker et al. 1990).

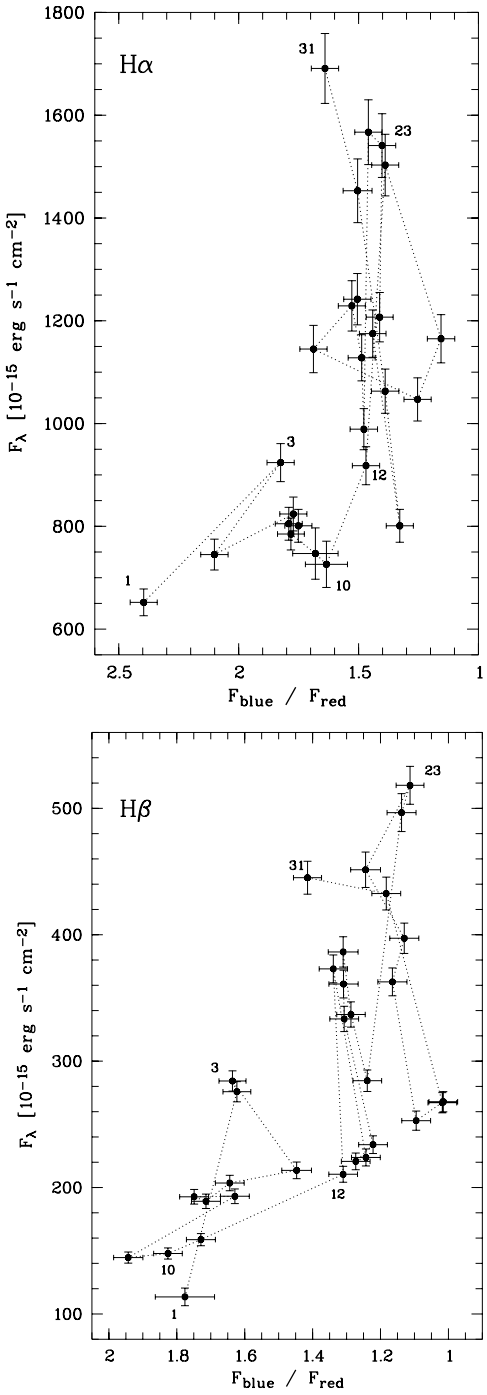

Fig. 11. Asymmetry-intensity plots of the Hα and Hβ profiles. Numbers denote individual observing epochs (see Table 2, remarks). Hα values are not available for all epochs.

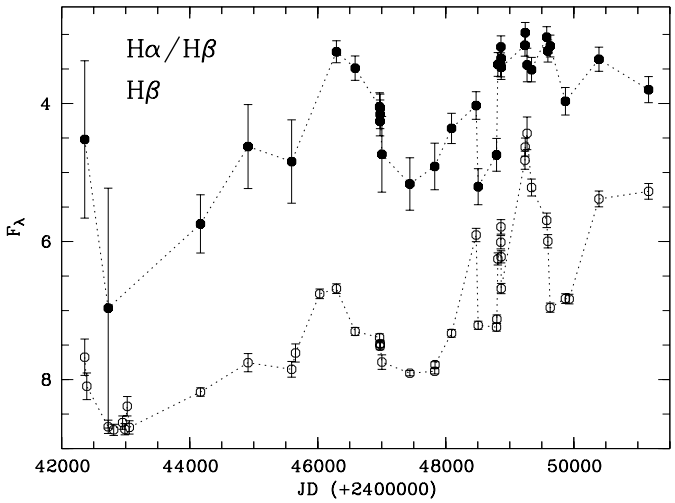

Fig. 12. The Balmer decrement Hα/Hβ as a function of time. For comparison a scaled Hβ light curve is shown (lower curve).

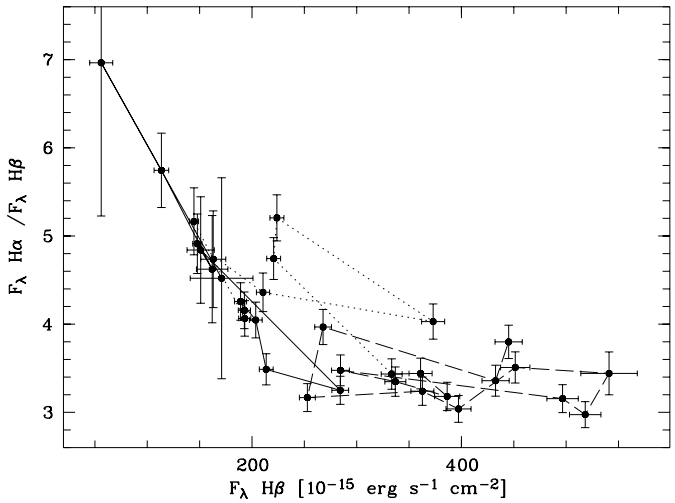

Fig. 13. The Balmer decrement Hα/Hβ as a function of Hβ intensity. The data are connected by a solid line until JD 2 448 090 and by a long dashed line from JD 2 448 814 on; the values in the intervening period are connected by a dotted line.

Goodrich (1995) obtained spectra of NGC 7603 in 1976 (low state), 1987 (high state) and 1993 (very high state) (see Table 2). He explained the spectral variations with reddening changes on time scales of a couple of years due to dust clouds passing in front of the nucleus of this object with tangential velocities of hundreds to thousands of km s^{-1}. But we observed considerable variations in the meantimes on time scales of years only (Table 2, Fig. 4). These short time scale variations can not be explained with dust clouds outside the broad-line region.

In Fig. 15 we plot the Hβ line asymmetry as a function of the Balmer decrement Hα/Hβ. There is a trend that the Hβ line asymmetry is correlated with the Balmer decrement from the beginning of the campaign until July, 1990 (filled circles). After July, 1992 the Balmer decrement did not vary much (open squares) and in the meantime (July, 1990 - July, 1992) the Balmer decrement varied nearly independently from line asymmetry. In this intervening period the Balmer decrement and the Hβ line intensity varied differently as well (see Fig. 13).

Until 1990 the strong Balmer decrement variations were mainly caused by variations in the red wing. Independent variations of the Balmer decrement in the red and blue line wings are hard to explain with collisional-excitation effects or simple optical depth effects.

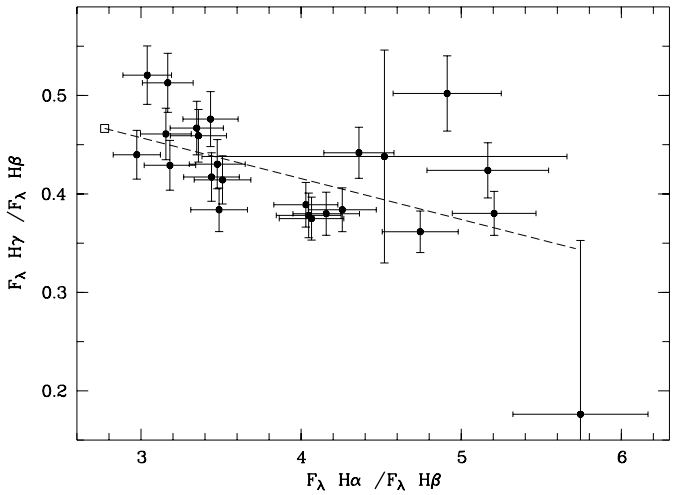

Fig. 14. Balmer line intensity ratios in NGC 7603 for different epochs. The open square shows the standard recombination ratio (case B). The dashed line shows the effects of standard interstellar extinction.

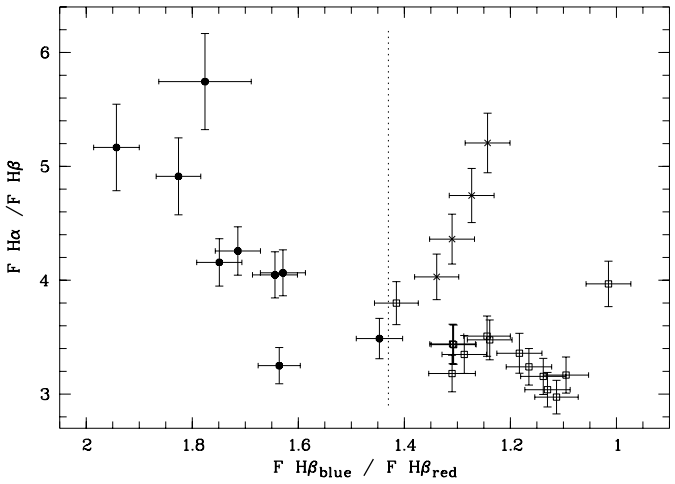

Fig. 15. Balmer decrement Hα/Hβ vs. Hβ line asymmetry. Observations earlier than JD 2 448 090 (July, 1990) are displayed as filled circles, observations later than JD 2 448 814 (July, 1992) are displayed as open squares and the data in the meantime are displayed as stars (see Fig. 9). The dashed line separates all observations made earlier than July, 1990.

To understand the observed variations one could speculate that NGC 7603 is a normal variable Seyfert 1 galaxy. In addition a thin foreground dust layer might be unevenly distributed in the line of sight - close to the emitting region - obscuring the emission of the red line wing more than the blue one. If the central ionizing source is in a low stage the BLR fills a smaller volume. In this case the relative foreground absorption is stronger compared to the high ionization stage with a larger BLR radius.

We probably can test the dust absorption model if the line intensities will decrease within the next years to the same level as before 1990. Then we can investigate the strength of line profile variations in different emission lines and verify whether the absorption or the geometry of the BLR has changed with time. We do not know yet if the observed emission lines are generated by photoionization in cloudlets - which are distributed more or less symmetrically - or if they are formed at the surface of an accretion disk (Murray & Chiang 1998).

4. Summary

NGC 7603 is one of the very few Seyfert galaxies spectroscopically monitored over a time interval of more than twenty years. There are considerable spectral variations on timescales of months to years. The light curves of the optical emission line intensities show stronger amplitudes compared to those of other Seyfert galaxies. The optical line intensities and the continuum varied by a factor of 5 to 10. It is remarkable that the variability amplitude of the broad optical FeII blends is of the same order as those of the Hα or HeI lines in this broad-line Seyfert 1 galaxy. Generally, the FeII lines vary hardly at all. It should be tested in a larger sample whether broad emission line Seyfert 1 galaxies vary stronger in FeII than narrow emission line Seyfert 1 galaxies.

The mean and rms profiles of the individual emission lines are different in this galaxy. The Balmer lines clearly show substructures in the rms profiles indicating geometrical inhomogenities or kinematic irregularities in the BLR.

There was a strong blue asymmetry in the Balmer lines at the beginning of our campaign in 1979 until 1990. During this period the line intensities where smaller compared to the rest of the campaign. Later on in the higher intensity stages the line profiles remained more or less symmetrically.

The Balmer decrement Hα/Hβ varied strictly anti-correlated with respect to the Hβ intensity until 1990. Later on the Balmer decrement showed only small scale variations in contrast to the Hβ line intensity variations.

The cause of the observed correlations of lower Balmer line intensity with stronger line asymmetry and steeper Balmer decrement during the first half of our campaign on the one hand and the cause for the change in the second half on the other hand are still unclear. This leads to the question whether the reasons are intrinsic variations in the BLR and/or surrounding dust absorption. It might be answered when the Hβ line intensity will decrease back to a lower intensity stage: then we can test if some physical conditions (size, geometry, obscuration) of the BLR might have changed or if the observed line variations are correlated with the Hβ intensity alone.

Acknowledgements. WK thanks the UT Astronomy Department for the warm hospitality during his long term visit. This work has been supported by a DAAD grant and by DFG grant Ko 857/13.

References

Arp H., 1971, ApL 7, 221
Bischoff K., Kollatschny W., 1999, A&A 345, 49
Brotherton M.S., Gregg M.D., Becker R.H., et al., 1999, ApJ 514, L61
Clavel J., Joly M., 1984, A&A 131, 87
Davidson K., Netzer H., 1979, Rev. Mod. Phys 51, 715
Dietrich M., Kollatschny W., Peterson B.M., et al., 1993, ApJ 408, 416

Gaskell C.M., Peterson B.M., 1987, ApJS 65, 1
Giannuzzo M.E., Stirpe G.M., 1996, A&A 314, 419
Goerdt A., Kollatschny W., 1998, A&A 337, 699
Goodrich R.W., 1989, ApJ 340, 190
Goodrich R.W., 1995, ApJ 440, 141
van Groningen E., Wanders I., 1992, PASP 104, 700
Kollatschny W., Dietrich M., 1996, A&A 314, 43
Kollatschny W., Dietrich M., 1997, A&A 323, 5
Kollatschny W., Fricke K.J., Schleicher H., et al., 1981, A&A 102, L23
Kollatschny W., Fricke K.J., 1985, A&A 146, L11
Kollatschny W., Goerdt A., 2000, in prep.
Kopylov I.M., Lipovetskii V.A., Pronik V.I., et al., 1974, Astrofizika 10, 305
Malkan M.A., Gorjian V., Tam R., 1998, ApJS 117, 25
Maoz D., Netzer H., Petersen B.M., et al., 1993, ApJ 404, 576
Murray N., Chiang J., 1998, ApJ 494, 125
Netzer H., Peterson B.M., 1997, In: Maoz D., Sternberg A., Leibowitz E.M. (eds.) Astronomical Time Series. Kluwer, Dordrecht, p. 85
Osterbrock D.E., 1977, ApJ 215, 733
Peterson B.M., Balonek T.J., Barker E.S., et al., 1991, ApJ 368, 119
Peterson B.M., 1993, PASP, 105, 247
Peterson B.M., Wanders I., Bertram R., et al., 1998, ApJ 501, 82
Rodríguez-Pascual P.M., Alloin D., Clavel J., et al., 1997, ApJS 110, 9
Rosenblatt E.I., Malkan M.A., Sargent W.L.W., et al., 1994, ApJS 93, 73
Rybicki G.B., Press W.H., 1992, ApJ 398, 169
Sharp N.A., 1986, ApJ 302, 245
Tohline J.E., Osterbrock D.E., 1976, ApJ 210, 117
de Vaucouleurs G., de Vaucouleurs A., Corwin H.G., et al., 1991, Third Reference Catalogue of Bright Galaxies
Wamsteker W., Rodríguez-Pascual P.M., Wills B.J., et al., 1990, ApJ 354, 446
Wanders I., Peterson B.M. 1996, ApJ 466, 174
Welsh W.F., Kollatschny W., Robinson E.L., 2000, Rev. Mex. Astron. Astrofis. in press
Wu C.-C., Boggess A., Gull T.R., 1983, ApJ 266, 28